Bioactive Materials 22 (2023) 168–179

Contents lists available at ScienceDirect

Bioactive Materials

journal homepage: www.keaipublishing.com/en/journals/bioactive-materials

Dynamic photoelectrical regulation of ECM protein and cellular behaviors

Xiaozhao Wang [b,c,d,e], Cai Yao [f], Xudong Yao [g], Junxin Lin [b,c,d,e], Rui Li [b,c,d,e], Kun Huang [a], Weiming Lin [a], Xiaojun Long [b,c,d,e], Chao Dai [d], Jiajun Dong [d], Xuegong Yu [a], Wenwen Huang [b,c,d,e], Wenjian Weng [a], Qi Wang [f], Hongwei Ouyang [b,c,d,e,*], Kui Cheng [a,**]

[a] School of Materials Science and Engineering, State Key Laboratory of Silicon Materials, Cyrus Tang Center for Sensor Materials and Applications, Zhejiang University, Hangzhou, 310027, China
[b] Dr. Li Dak Sum & Yip Yio Chin Center for Stem Cells and Regenerative Medicine, Department of Orthopedic Surgery of the Second Affiliated Hospital, Zhejiang University School of Medicine, Hangzhou, 310058, China
[c] Department of Sports Medicine, Zhejiang University School of Medicine, Hangzhou, 310058, China
[d] Zhejiang University-University of Edinburgh Institute, Zhejiang University School of Medicine, Key Laboratory of Tissue Engineering and Regenerative Medicine of Zhejiang Province, Zhejiang University School of Medicine, Hangzhou, 314400, China
[e] China Orthopedic Regenerative Medicine Group (CORMed), Hangzhou, 310058, China
[f] School of Chemistry, Zhejiang University, Hangzhou, 310027, China
[g] International Institutes of Medicine, The Fourth Affiliated Hospital, Zhejiang University School of Medicine, No. N1, Shangcheng Avenue, Yiwu, 322000, China

ARTICLE INFO

Keywords:
Graphene
Protein conformational change
Charge transfer
Cell-materials interaction
n-doping

ABSTRACT

Dynamic regulation of cell-extracellular matrix (ECM)-material interactions is crucial for various biomedical applications. In this study, a light-activated molecular switch for the modulation of cell attachment/detachment behaviors was established on monolayer graphene (Gr)/n-type Silicon substrates (Gr/Si). Initiated by light illumination at the Gr/Si interface, pre-adsorbed proteins (bovine serum albumin, ECM proteins collagen-1, and fibronectin) underwent protonation to achieve negative charge transfer to Gr films (n-doping) through π-π interactions. This n-doping process stimulated the conformational switches of ECM proteins. The structural alterations in these ECM interactors significantly reduced the specificity of the cell surface receptor-ligand interaction (e.g., integrin recognition), leading to dynamic regulation of cell adhesion and eventual cell detachment. RNA-sequencing results revealed that the detached bone marrow mesenchymal stromal cell sheets from the Gr/Si system manifested regulated immunoregulatory properties and enhanced osteogenic differentiation, implying their potential application in bone tissue regeneration. This work not only provides a fast and feasible method for controllable cells/cell sheets harvesting but also gives new insights into the understanding of cell-ECM-material communications.

1. Introduction

Cells continually sense and respond to physicochemical cues in the extracellular environment via specific sensors when in contact with materials [1–3]. Cellular adhesion is the initial yet crucial step, considering it transduces external physicochemical signals into cells through the anchoring site to the cellular receptor [4]. Dynamically regulating cell adhesion behaviors is critical to direct cell behaviors and fates, thereby holding profound potential in many biomedical applications, ranging from cell-based therapy and immunotherapy to tissue engineering [5–8]. To date, switchable control strategies by shifting the surface properties "on" or "off" with external stimuli have attracted considerable attention in control over cell adhesion [9–13]. Among them, light-responsive surfaces are most preferred owing to their high spatiotemporal precision [13–16].

Photo-switching approaches involving photosensitive molecules

Abbreviations: graphene, Gr; silicon, Si; extracellular matrix, ECM; bone marrow mesenchymal stem cells, BMSCs; fibronectin, Fn; bovine serum albumin, BSA; collagen-1, Col-1.

Peer review under responsibility of KeAi Communications Co., Ltd.

* Corresponding author. Dr. Li Dak Sum & Yip Yio Chin Center for Stem Cells and Regenerative Medicine, Department of Orthopedic Surgery of the Second Affiliated Hospital, Zhejiang University School of Medicine, Hangzhou, 310058, China.
** Corresponding author.
E-mail addresses: hwoy@zju.edu.cn (H. Ouyang), chengkui@zju.edu.cn (K. Cheng).

https://doi.org/10.1016/j.bioactmat.2022.09.022
Received 6 June 2022; Received in revised form 7 September 2022; Accepted 21 September 2022

undergoing degradation, isomerization reactions, and photothermal responses triggered by UV or NIR light have been validated as viable options by which cell adhesion and release can be controlled on demand [2,10,13,16]. Although promising, these systems exert functions indirectly by eliciting changes in exogenous chemical molecules rather than directly modulating behaviors of extracellular matrix (ECM) proteins. This is mainly attributed to the fact that ECM signals are complicated to be activated and controlled on purpose [17]. Nevertheless, the chemical residuals, high light power, as well as photothermal effects in these photo-switchable systems would generate opposite effects on detached cells and thus limit their subsequent phenotypes [10,18,19]. Given these considerations, a noninvasive light source along with a light-responsive substrate is desirable for mediating the behaviors of cell adhesion protein families without giving extra rise to local changes (pH, temperature, etc.).

Our previous work provided a strategy for visible light-regulated cell detachment based on Si(p/n) (silicon substrate with p/n junction) [20]. Due to its biologically friendly nature, visible light has proven to be an ideal option. Without introducing additional chemical molecules, the photogenerated electrons accumulated on the surface exerted repulsive forces on the ECM proteins, thereby leading to efficient cellular detachment [20]. Surface charge properties are reported to intensively affect protein adsorption behaviors, such as their composition, distribution, and conformations, by which cell behaviors are dynamically regulated [21–25]. As the protein itself possesses variously charged residues [26], a candidate surface that is not only sensitive to the charge variation through specific interactions when the protein is adsorbed but also offers dynamic regulation of such interactions by visible light illumination, could be potentially applicable in the dynamic regulation of cell adhesion behaviors. In this case, Graphene/n-Si (Gr/Si) substrates are prioritized owing to the three merits: To begin, the Schottky junction formed between Gr and n-Si allows the substrates to absorb visible light and generate holes accumulation in the Gr layer, resulting in tuned surface charge properties [27]; Secondly, due to the zero bandgap, Gr carrier densities could be easily modulated via surface adsorption (like organic molecules and protein), exhibiting n-type and p-type doping [28]; Lastly, the intrinsically hydrophobic nature of Gr endows it with the ability to interact with proteins through noncovalent binding (hydrogen bond or π-π stacking interactions) [29–31]. The latter of which could facilitate charge transfer between protein and Gr without impacting the Gr structure and further the light response of Gr/Si, thereby providing favorable regulation of protein-material interactions [32–34]. In addition, our previous study demonstrated that appropriate light-induced charge accumulation on the Gr/Si surface could enhance osteogenic differentiation of bone marrow mesenchymal stem cells (BMSCs), which further the potential applications of Gr/Si in biomedical fields like bone regeneration [35].

Taking these advantages of Gr/Si, herein, by regulating the conformations of ECM proteins through special interactions of protein-Gr/Si by visible light illumination, a facile yet versatile strategy for controlling cell adhesion/detachment behaviors noninvasively was given. The mechanism underlying how ECM proteins interacted with Gr/Si upon light illumination was studied by experimental analysis and molecular dynamics (MD) simulation [35]. The properties of single cells/cell sheets harvested with visible light illumination were further investigated.

2. Experimental section

2.1. Preparation and characterization of graphene/silicon substrates

The graphene/silicon (Gr/Si) substrates were fabricated as described previously [27]. N-type Si (0.05 Ω cm< resistivity<0.1 Ω cm, 300 μm thick, <100>) wafers and glass were used as the substrates to fabricate the Gr/Si substrates. Briefly, the Si wafers were ultrasonically cleaned in deionized water and diluted HF solution (1:50, v-v) for several min to remove the native oxide, and dried in N_2 for further utilization. The commercially available monolayer Gr (Nanjing XFNANO Materials Tech Co., Ltd) was firstly cut into squares (10 mm × 10 mm), then spin-coated with the polymethyl methacrylate (PMMA) at 6000 rpm for 60 s, followed by curing at 90 °C for 5 min. After that, the Cu foil on the backside of Gr was etched away using an ammonium persulfate aqueous solution (1 M). The resulting Gr films were rinsed with deionized water several times, then transferred onto the as-prepared Si or glass substrates, and finally soaked in acetone to remove the PMMA. All samples were ultrasonically cleaned in deionized water for several min for further cell experiments. The surface topography features of the samples were detected by atomic force microscopy (AFM, NTEGRA Spectra, NTMDT). The water contact angles (WCA) were measured using a contact angle meter (Dataphysics, OCA20). X-ray photoelectron spectroscopy (XPS, Kratos AXIS Ultra DLD, Al Kα, 1486.6 eV) and Raman spectroscopy were carried out to estimate the quality of graphene. To analyze the photovoltaic characteristics of the samples, patterned Au electrodes were deposited on the surface of Gr, and the InGa eutectic alloys were spin-coated for the back contacts. The characteristics of Gr/Si were measured by a Keithley 2400 source meter under standard test conditions (AM 1.5, T = 300 K, and p = 100).

2.2. Protein adsorption behaviors

XPS with an Al Kα source (1486.6 eV) was used to investigate the evolution of protein status adsorbed on the Gr/Si surface before and after visible light illumination. C1s at 284.6 eV was used for calibration. Detailed N1s and C1s were carried out with a step of 0.1 eV. Bovine serum albumin (BSA), collagen-1 (Col-1), and fibronectin (Fn) were used as model proteins. Attenuated total reflectance Fourier transform infrared spectroscopy (ATR-FTIR, Thermo Fisher, Nicolet 5700) was used to measure the conformational changes of protein adsorbed. Micro-Raman spectroscopy was performed to measure the doping process between adsorbed proteins and Gr/Si using a confocal Raman microscope equipped with a 532 nm laser. (LabRAM HR Evolution, Horiba Co., Ltd.).

2.3. MD simulation

The Gr sheet was constructed by the graphene online creation server [36]. The electric field (corresponding to different photovoltages) exerted on the system was calculated from the Gouy-Chapman-Stern (GCS) model [20,37]. The initial structures of BSA and FN-$III_{9\text{-}10}$ were taken from Protein Data Bank entries $4F5S^{8}$ and 1FNF [38,39]. respectively, followed by 50 ns equilibration. BSA was considered as a triangular prism with 5 orientations, and FN-$III_{9\text{-}10}$ was treated as a cuboid with 6 orientations due to the geometric irregularity. Each orientation of BSA and FN-$III_{9\text{-}10}$ was placed at a distance of 1.0 nm from the Gr sheet along the z-direction. Then, different configurations were equilibrated by 200 ns MD to select the most stable conformation of BSA or FN-$III_{9\text{-}10}$ on the Gr surface. After that, an electric field with 0.12 V/nm (corresponding to 0.40 V voltage) in the z-direction was subsequently applied to all systems to study the conformational changes of protein adsorbed. All simulations were performed with GROMACS 5.0.4 package [40] using the AMBER99SB-ILDN force field [41]. The bond lengths were constrained by the LINCS algorithm [42] and periodic boundary conditions were applied in all directions. The cut-off of van der Waals interaction was 1.2 nm. The particle mesh Ewald (PME) summation [43] was used to calculate the long-range electrostatic interaction with a truncation distance of 1.2 nm. The simulated box measuring 13.34 × 13.44 × 12.00 nm^3, was solvated and neutralized by 0.15 mol/L NaCl solution. All simulations were carried out in the NVT with a time step of 2 fs. The temperature was controlled at 298 K by the modified Berendsen thermostat coupling method. The electric field (corresponding to light illumination) exerted on the system was calculated from the Gouy-Chapman-Stern (GCS) model [20,37].

2.4. Cell culture

MC3T3-E1 cells were cultured in alpha minimum essential media (α-MEM) supplemented with 10% fetal bovine serum (FBS, Gibco), 10000 mg/mL penicillin, and 10000 mg/mL streptomycin (Gibco), 1% MEM nonessential amino acids (Gibco), and 1% sodium pyruvate (Gibco) in a humidified atmosphere of 5% CO_2 at 37 °C. After reaching confluency, the cells were harvested using 0.25% trypsin/EDTA (Gibco) for the next experiments. Rat bone marrow mesenchymal stromal cells (rBMSCs) were isolated from the bone marrow of femurs and tibias of three-week-old male Sprague-Dawley rats according to a protocol approved by the Institutional Animal Care and Use Committee of Zhejiang University, Hangzhou, China. Then, they were cultured in Dulbecco's modified Eagle's medium (Gibico) containing 10% fetal bovine serum (Gibco), 0.272 g/L L-glutamine (Sigma), and 1% antibiotic solution (penicillin and streptomycin (Gibco)). BMSCs were used between the third and fifth passage. The cells were cultured on Gr/Si surface at different densities according to various experiments: 5×10^4 cells/cm^2 for single cell detachment assay or 1×10^5 cells/cm^2 for cell sheets related experiments.

2.5. Cell detachment assay

After culturing MC3T3-E1 cells on the substrates for 24 h, they were examined for visible light-controlled release. Visible light (50 mW/cm^2) was illuminated on the samples for 0, 3, 5, and 10 min, respectively, and the substrates were gently rinsed with phosphate-buffered saline (PBS) thrice to remove the detached cells. Then, it was measured with 4′-6-diamidino-2′-phenylindole (DAPI, 2 μg mL^{-1} in PBS) staining to monitor the cell release. To examine the selective detachment of adhered cells, graphene films with smaller areas were transferred onto the Si surface. The same cell detachment assay was performed on such Gr/Si substrates. And the local cell detachment was measured by fluorescence staining with DAPI and calcein-AM. After culturing MC3T3-E1 cells for 5 days, the cells were confluent. Then, they were illuminated with visible light (50 mW/cm^2) for 10 min to release from the substrate. BMSCs cell sheets could also be harvested by the same light treatments.

2.6. Characterization of harvested cells/cell sheets

After single-cell detachment, the released MC3T3-E1 cells were collected and incubated with Annexin V-fluorescein isothiocyanate (FITC, 0.1 mg/mL) and propidium iodide (PI; 0.5 mg/mL) for cell viability analysis. To analyze the re-adhesive properties of the detached cells, they were collected and re-seeded on the new culture plates. After culturing for 24 h, cells were fixed and washed with PBS, then permeabilized with 0.1% Triton X100, and blocked in PBS solution with 2.5% BSA (Sigma) and 10% FBS (Gibco) for 60 min at room temperature. The mouse anti-vinculin antibody (Abcam) was used for the primary antibody. The fluorescent dye, FITC-488 conjugated phalloidin, was used for cytoskeleton staining. The secondary antibody was Alexa Fluor-conjugated secondary antibody, and the nuclei were stained with DAPI. The cells were observed by confocal laser scanning microscopy (Nikon A1 Ti, Tokyo, Japan). Trypsinized cells were used as the control.

As for the harvested cell sheets, their viability was assessed with live/dead staining. Briefly, after washing with PBS thrice, the calcein-AM and PI dyes were added to the detached cell sheets and incubated for 15 min at 37 °C. Finally, the cells were imaged using a fluorescence microscope. To observe the cell-cell connection, Alexa Fluor 488 anti-pan cadherin antibody (Abcam) was used for immunostaining the detached cell sheets. The cytoskeleton of cell sheets before and after release was stained with FITC-488 conjugated phalloidin. The samples were imaged by a confocal laser scanning microscopy (Nikon A1 Ti, Tokyo, Japan). The integrin and retention of ECM proteins in detached cell sheets, including integrin-β1, Col-1, Fn, and laminin (LN) were measured by immunostaining. Their primary antibodies were goat anti-integrin-β1 (Invitrogen), mouse anti-Col-1 antibody (Abcam), rabbit anti-LN antibody (Abcam), and mouse anti-FN antibody (Abcam). The secondary antibodies were FITC 488-conjugated donkey anti-goat, Alexa Fluor 488-conjugated goat anti-mouse and Alexa Fluor 594-conjugated donkey anti-rabbit (Jacson Immuno Research, Inc.). The nucleus was stained with DAPI. Finally, the samples were visualized by confocal laser scanning microscopy (Nikon A1R/A1).

The alkaline phosphatase (ALP) activity of harvested cell sheets was measured using an ALP activity assay according to the manufacturer's procedure (Wako, Japan). ALP color development kit (Beyotime, China) was used to stain the ALP product. The expression levels of osteogenic differentiation-related genes of MC3T3-E1 were measured using real-time polymerase chain reaction (RT-PCR). After cell sheet detachment, RNA was extracted by the TRIzol reagent. Then, the RT-PCR analysis was performed on a Roche LightCycler 480 system with an SYBR Green I matermix. The expression levels of target genes were normalized to that of glyceraldehyde-3-phosphate dehydrogenase (GAPDH). The primers were tabulated in table S7. Cell sheets cultured on PS plates were used as the control. To measure the migration properties of harvested cell sheets, the fragments of detached cell sheets were reseeded onto a new 24-well plate and cultured for 1 day, 3 days, and 5 days. At the designed time point, the outgrowth of cells from fragments was detected using cytoskeleton and vinculin staining.

RNA-seq and data analysis. RNA-seq was performed according to a previous study [44]. Briefly, the total RNA was extracted from the rBMSCs cell sheets harvested from Gr/Si before and after light illumination, and cells cultured on PS plates using TRIzol reagent (n = 3). The reverse transcription was performed using SuperScript II reverse transcriptase (Invitrogen). Double-strand cDNA was conducted using NEBNext mRNA second strand synthesis kit (NEB), and double-strand DNA was cleaned with AMPure XP beads (Beckman Coulter). The sequencing library was constructed with high-quality RNA samples using Nextera XT kit (Illumina, San Diego, CA)) and sequenced on the Illumina X-Ten platform. Hisat2 (https://ccb.jhu.edu/software/hisat2/index.shtml) software was used to map the Sequence reads with the default parameter, and HTSeq was used for genes read (https://htseq.readthedocs.io/en/release_0.11.1/). DESeq2 was applied to identify differentially expressed genes [45]. Differentially expressed genes (DEGs) were chosen as foldchange of greater than 2 and padjst value of less than 0.05. Gene ontology analysis was performed using DAVID and REVIGO (https://david.ncifcrf.gov; http://revigo.irb.hr/).

2.7. Statistical analysis

All data were expressed as mean ± standard deviation (n = 3). Statistical analysis was determined via Student's t-test and one-way ANOVA. Values of $^*p < 0.05$ was considered statistically significant.

3. Results and discussion

3.1. Photoelectrical properties of Gr/Si substrates

With the polymethyl methacrylate-assisted wet transfer method, chemical vapor deposition-grown monolayer Gr films were coated conformally onto the n-Si substrates [35,46]. Fig. 1a showed the Raman spectrum of Gr on n-Si substrates. The negligible defect-related D band at around 1350 cm^{-1} as well as the sharp and symmetric 2D band of Gr/Si substrate indicated the monolayer Gr film of high quality [47,48]. The atomic force microscopy (AFM) image of Gr/Si revealed the typical wrinkled topography of Gr (inset) [49]. Furthermore, WCA results illustrated the hydrophobic nature of Gr on the Si substrate (Fig. 1b) [50]. These characteristics indicated the successful transfer of the Gr film onto the n-Si wafer, resulting in a Schottky junction at the Gr/Si interface. Afterward, the photovoltaic properties of Gr/Si were evaluated. The open-circuit voltage (V_{OC}) of the Gr/Si substrate was 0.396 V, exposing the effects of heterojunction of Gr/Si (Fig. 1c and Fig. S1). This

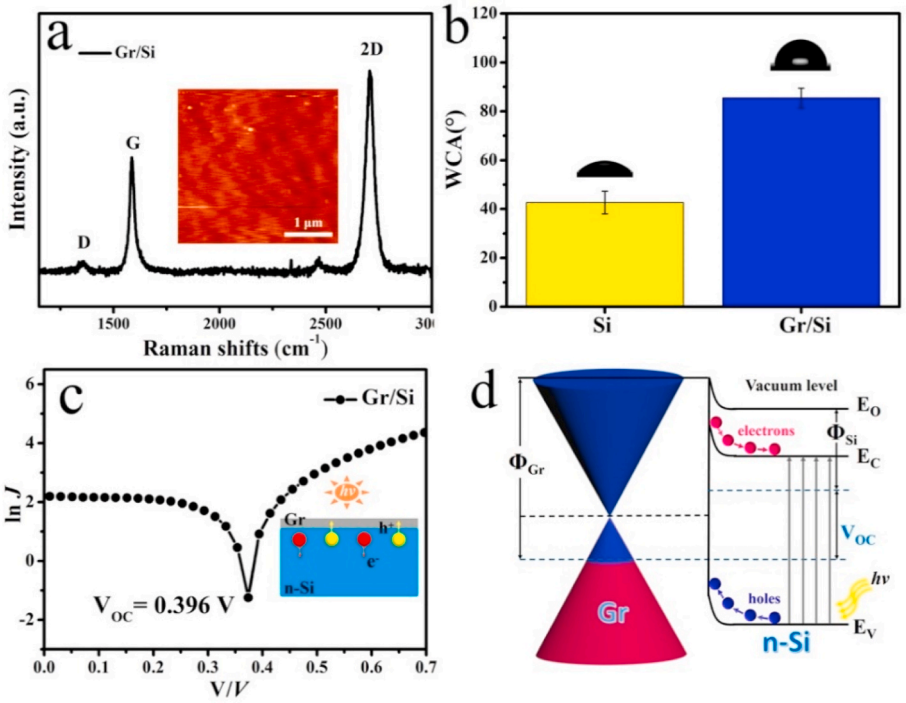

Fig. 1. Photoelectrical properties of Gr/Si substrate. (a) Raman spectrum of Gr/Si substrate. Inset: AFM image of Gr/Si surface, scale bars are 1 μm; Water contact angles of Gr/Si substrate and bare Si wafer; (c) *I–V* characteristic of Gr/Si substrate showing its photovoltaic effects. Inset: schematics of the light-induced charge separation of Gr/Si; (d) Band energy diagram of Gr/Si Schottky junction upon light illumination.

junction formed at the interface between Gr and n-Si produced a built-in field and separated the photo-generated carriers [27]. With high transparency and carrier mobility, the Gr film atop n-Si allowed visible light transmission and was favorable to charge separation and hole transport [51]. As a result, photo-generated holes were diffused across the junction and swept to the Gr side, conferring positive charge accumulation in the Gr film (Fig. 1c inset and 1d) [34]. When the light intensity was increased above 50 mW/cm^2, the V_{OC} of Gr/Si was saturated [35], suggesting that the photovoltaic effects were maximized in agreement with our previous work [20]. Though light-induced charge accumulation on Gr/Si surface, it nearly did not affect the WCA of the Gr/Si surface (Fig. S2). Herein, a visible light-responsive platform with tunable surface charge properties was fabricated.

3.2. *Light-induced charge transfer from adsorbed protein to Gr/Si via photovoltaic interface*

The cell-material interactions were driven by the evolution of the pre-adsorbed protein [20,52], which could be modulated by surface charge [23]. Thus, considering the light-induced charge accumulation properties of Gr/Si, experimental analysis and MD simulation were subsequently conducted to provide insights into the mechanism underlying the interaction between protein and Gr/Si surface with light illumination. Taking into account that BSA was the most abundant protein in the serum, it was selected as one of the model proteins to simplify the protein model [20,53]. The chemical status of BSA adsorbed on Gr/Si before and following light illumination was monitored by X-ray photoelectron spectroscopy (XPS) (Fig. 2a–f). Before light illumination, evident adsorption of BSA on the Gr/Si surface (Gr/Si-BSA) was confirmed, as indicated by the emergence of nitrogen signal (Fig. 2a), an increase in the nitrogen-to-carbon (N/C) ratio (Fig. 2b), and the presence of chemical functional groups (carbon/nitrogen-containing groups) (Fig. 2c and d). After illuminating with light, decreases in nitrogen peak and N/C ratio were observed on light-illuminated samples (Gr/Si-BSA-Light), suggesting a relatively lower amount of BSA adsorbed (Fig. 2e and f). In C1s spectra (Fig. 2e), the content of initial peaks of Gr/Si-BSA-Light samples showed great changes. Notably, new protonated NH_3^+ groups (content: 8.9%) emerged on Gr/Si-BSA-Light samples (Fig. 2f), with the peak representative of unprotonated $–NH_2$ being increased by 3.8% and deprotonated –NH decreased by 12.7%. This observation evinced that light illumination could give rise to amino protonation for adsorbed residues of BSA on Gr/Si.

Previous studies have described that protein molecules underwent protonation or deprotonation to act as electron donors or acceptors on the Gr/Si surface to tune p- or n-type doping of Gr/Si [28,31,54]. It implied that electrons from negatively charged residues of BSA molecules diffused to Gr/Si via the photovoltaic interface (Schottky junction) [28,54]. The charge transfer doping properties afforded by BSA molecules on the Gr/Si surface were further studied by Raman spectroscopy. As displayed in Fig. 2g, the G band peak frequencies of Gr/Si-BSA and Gr/Si-BSA-Light were determined to be 1574 cm^{-1} and 1567 cm^{-1}, downshifted by 13 and 19 cm^{-1} from that of bare Gr/Si (1587 cm^{-1}), inferring that n-type doping of Gr was caused by BSA adsorption and further enhanced with light illumination [28,31,55]. [56,57]. When using ECM protein, Fn as a model protein, the G band peak of Gr/Si-Fn was shifted from 1588 cm^{-1} to 1578 cm^{-1} (Gr/Si-Fn-Light) after light illumination (Fig. 2h), which was consistent with the BSA results. Such effects were further validated by the decreased ratio in the intensities of the 2D and G bands (I(2D)/I(G)) (Fig. S3). Its downshifting could be ascribed to the electron transfer from protein molecules to Gr/Si by π-π interactions [28,58,59]. However, BSA and Fn adsorbed on the non-light-responsive Gr/Glass substrates did not show a similar light-regulated electron-doping process to Gr/Si substrate (Fig. S4). Thus, charge transfer from protein molecules to the Gr/Si could be modulated by light illumination [34], and this light-regulated doping process may further disrupt secondary structures of protein and concurrently induce conformation changes in protein (Fig. 2i) [60,61].

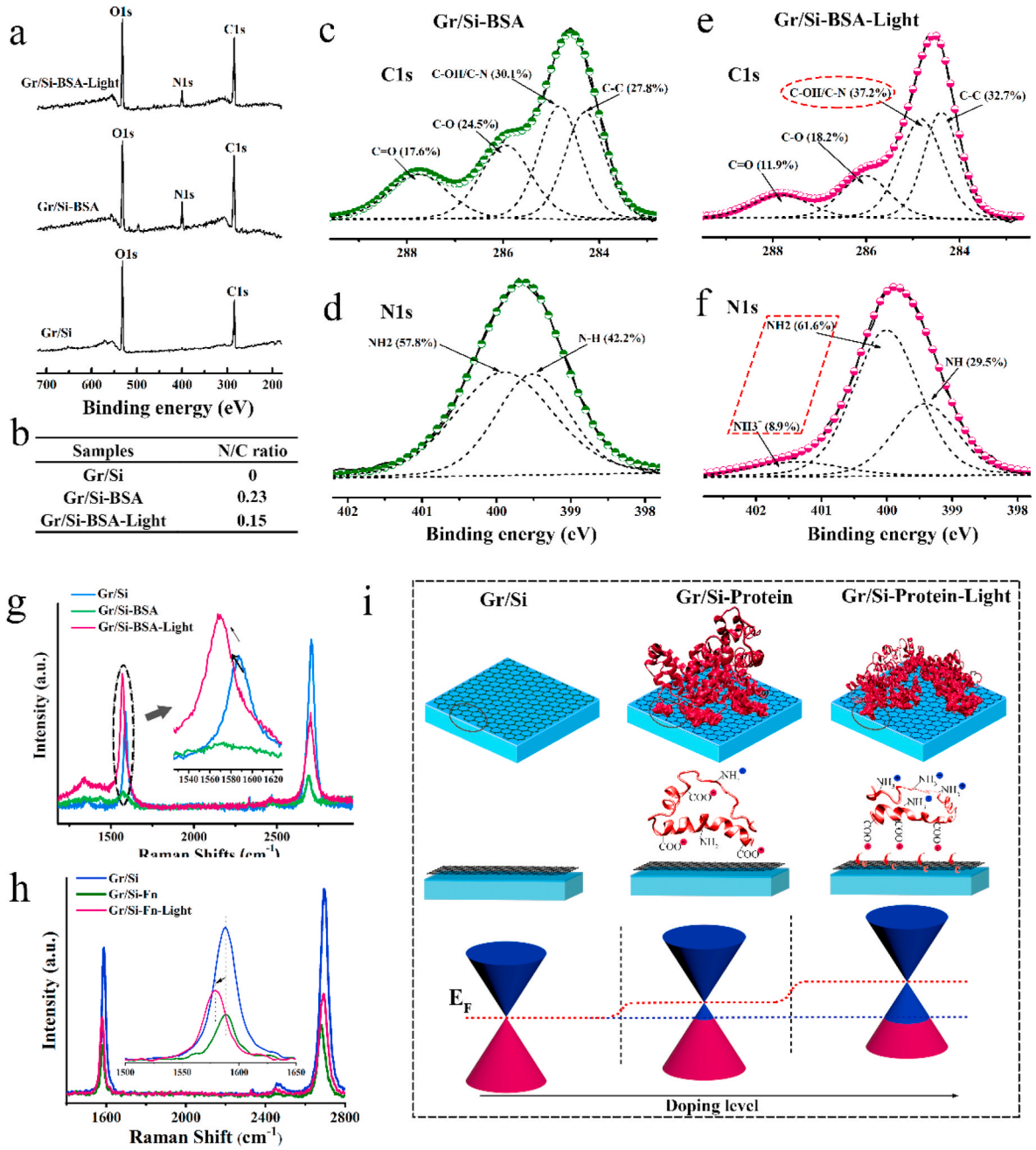

Fig. 2. Light-induced charge transfer from adsorbed protein to monolayer Gr via Gr/Si photovoltaic interface (Schottky junction). (a) and (b) are XPS survey spectra and N/C ratio of bare Gr/Si, Gr/Si-BSA, and Gr/Si-BSA-Light surfaces; (c–f) are C1s and N1s high-resolution spectra of Gr/Si-BSA and Gr/Si-BSA-Light surfaces, respectively. Notably, the content of C═O and C–O were reduced by 5.7% and 6.3%, respectively, and that of the electron-rich groups, C–OH/C–N, was increased by 7.1% after light illumination; (g) and (h) are Raman spectra of BSA-Gr/Si and Fn-Gr/Si substrates before and after light illumination comapred with bare Gr/Si substrate; Inset was the amplified spectra showing the changes of G band position; (i) Illustration showing protein-Gr/Si interactions regulated by light illumination. With light illumination, negative charges transferred from protein to Gr/Si substrate, resulting in changes in their original adsorption status and Gr band structure.

3.3. Light-induced charge transfer drives conformational changes of adsorbed protein on Gr/Si

To evaluate light-induced conformational changes of the protein adsorbed on Gr/Si, Fourier transform infrared spectroscopy (FTIR) was carried out. Secondary structures of BSA, Col-1, and Fn adsorbed on the Gr/Si surface modulated with light illumination were calculated by deconvoluted curve-fitting of the amide I band (Fig. 3a–f, Fig. S5-S7) [62]. In the case of BSA and Fn adsorption (Fig. 3a–f), apparent peak shifting (Fig. S5 and S6) was detected with light illumination, clearly indicating the variation in secondary structure stimulated by light illumination. After calculation analysis, α-helix (35.2%) and β-sheet (32.2%) were found to be the predominant secondary structure of BSA adsorbed on Gr/Si before light illumination (Fig. 3c), while both contents considerably decreased, and the unordered structure β-turn (55.3%) and random coil (20.4%) became the primary contents after light illumination. It is worthwhile pointing out that the WCA of Gr/Si-BSA was slightly elevated following light illumination, indicating more hydrophobic residues were exposed (Fig. S8). These results suggested that light illumination could induce a conformational transition of BSA adsorbed on Gr/Si from an ordered to an unordered structure. Similar trends in conformational variation were further demonstrated

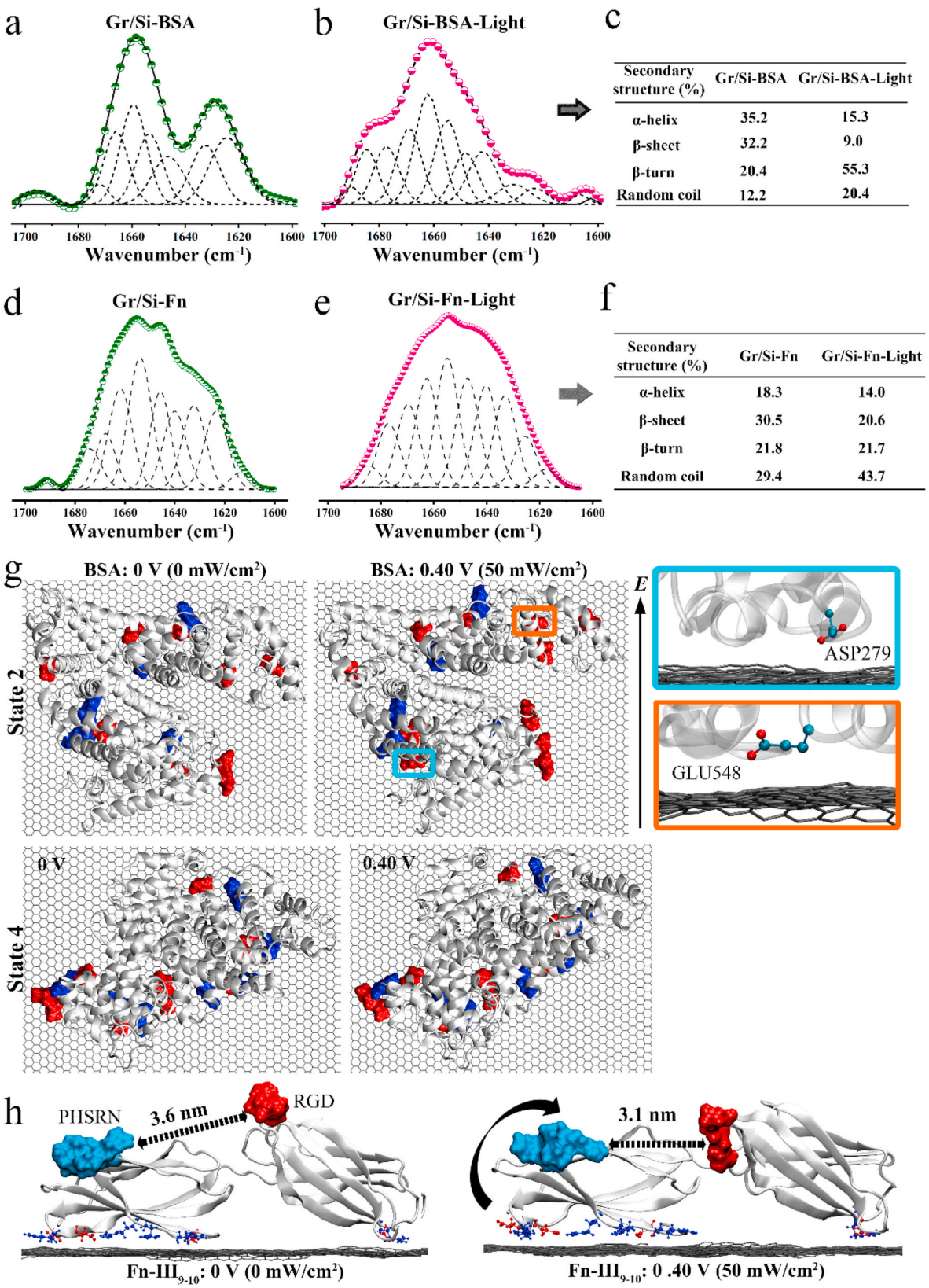

Fig. 3. Light-induced charge transfer drives conformational changes of adsorbed protein on Gr/Si surface. (a–b) FTIR absorbance in the amide I band for Gr/Si-BSA and Gr/Si-BSA-Light surfaces. Deconvoluted peaks representative of secondary structures for BSA were shown below both curves; (c) The relative contents of secondary structures of BSA for both surfaces; (d–e) FTIR spectra of Fn adsorbed on Gr/Si before and after light illumination; (f) Secondary structures of Fn adsorbed on Gr/Si before and after light illumination. (g–h) Conformations of BSA and Fn-III$_{9\text{-}10}$ adsorbed on Gr surface with 0 V and 0.40 V voltage after 200 ns MD simulation. Red and blue represented the acidic residues and basic residues of BSA molecules that interacted with Gr, respectively. Two more acidic residues of BSA, Asp279, and Glu548, were found to interact with Gr closely with 0.40 V voltage.

by Col-1 and Fn adsorbed on Gr/Si modulated with light illumination (Fig. 3d–f, Fig. S6, and S7). While, these proteins adsorbed on non-active Gr/Glass did not exhibit light-induced changes in secondary structures (Fig. S9), which further consolidated the light-mediated protein adsorption behaviors on Gr/Si surface. Although great conformational changes of proteins on Gr/Si happened, the corresponding adsorption amounts of BSA, Col-1 and Fn, respectively, showed little decrements by light treatment (Fig. S10), also suggesting light illumination determined the protein conformational changes on Gr/Si surface.

Regardless of serum protein BSA or ECM proteins (Col-1 and Fn), they may undergo protonation to donate charge to Gr/Si through π-π interactions (Fig. 2) [34,54], resulting in their conformational changes (Fig. 3a–f, Fig S5-S8). This implied that other ECM proteins may also possess similar light-regulated adsorption behaviors on Gr/Si.

To elucidate these light-regulated protein adsorption behaviors at the molecular level, MD simulations were further performed (Fig. 3g and h) [20]. To corroborate the above experimental analysis, BSA was first used as the model protein [63]. After 200 ns MD simulation, binding states 2 and 4 of BSA on Gr were found to have relatively stable conformations, with the latter having a relatively higher van der Waals interaction energy (E_{vDW}) and was considered the preferred conformation (Fig. 3g, S11, and Table S2). After applying a 0.40 V voltage (light intensity, 50 mW/cm^2) to the system, the optimal conformation of BSA was shifted to state 2, which contained 11 acidic and 5 basic adsorbed residues intimately interacting with Gr and showed greater affinity adsorption compared with state 4 (Fig. 3g, S11c, Table S3, and Table S4). This indicated optimal conformations of BSA adsorbed on Gr showed significant differences with various voltages, in line with the experimental results in Fig. 3a–c. Besides, the content of hydrophobic residues that closely interacted with Gr was directly exposed outwardly (measured at 0.8 nm from Gr surface) for state 2 and increased from 24% to 26% and 26%–30% with a 0.40 V voltage, respectively, which is consistent with Fig. S8. Such increment could enhance π-stacking interactions between Gr and BSA due to the hydrophobic nature of Gr [55,64]. As the voltage exerted attractive and repulsive forces on acidic and basic residues, respectively, the van der Waals interaction between BSA and Gr should be the driving force for the conformational changes of BSA (Table S3 and S4) [65–67].

Available conformations of Fn have been recognized to play a key role in harnessing cell adhesion behaviors via controlled binding with the integrin family [68]. Therefore, the behavior of Fn molecules on Gr/Si surfaces with differing voltages is crucial for elucidating light-regulated cell-material interactions. Next, the Fn-$III_{9\text{-}10}$ domain with integrin-binding motif (RGD) and synergy site (PHSRN) was selected as the model to investigate in MD simulation (Fig. 3h) [69,70]. After 200 ns MD simulation, Fn-$III_{9\text{-}10}$ could be stably adsorbed on the Gr surface with adequate RGD exposure and a proper distance of 3.6 nm between the RGD and PHSRN (Fig. S12, Table S5). When a 0.40 V voltage was applied, though the initially adsorbed residues were unaltered, their interactions with Gr and the original conformation did, leading to a loss in overall stability (Table S6, Table S7, Video S1). RGD motif was likely to be hidden inside the protein due to the formation of ion pairs between Arg in RGD and Glu residues (Video S1). The distance between RGD and PHSRN was reduced to 3.1 nm, which may also show an opposite effect on cell adhesion [71]. These conformational changes should mainly originate from the van der Waals interaction between protein and Gr [67], which was weakened with the 0.40 V voltage. Appropriate conformation of Fn with satisfactory exposure of RGD and a ~3.5 nm distance between RGD and PHSRN could maximize its recognition by integrin and thus facilitate cell adhesion [72]. The conformation alterations of Fn-$III_{9\text{-}10}$ on Gr with a 0.4 V voltage could adjust the full binding between integrin and RGD to partial binding, subsequently affecting cell adhesion [73]. MD simulation further demonstrated that conformational protein changes occurred on the Gr/Si surface in a light-regulated fashion.

3.4. Light-induced controlled cell detachment from Gr/Si surface

The effective bindings of integrin-β1 to ECM proteins, like α1β1 to collagen and α5β1 to fibronectin, play a role in mediating cell adhesion [74]. In our system, light-regulated efficient charge transfer from ECM proteins to Gr/Si induced conformational changes in the protein adsorbed (Figs. 2 and 3) [34,54,55,75]. In this process, the specific recognition between ECM proteins (such as Fn, not limited) and integrins (cell adhesion receptor) may be affected (Fig. 3), thus affecting cell adhesion behaviors [20–25]. Regarding its applications, the ability of Gr/Si for regulating cell detachment behaviors with visible light illumination was investigated (Fig. 4). Firstly, visible light-controlled single-cell detachment on Gr/Si was assessed. Schematics in Fig. 4a depict this process. Before light illumination, MC3T3-E1 preosteoblasts were cultured on Gr/Si surface as a model. Considering the maximized variation of surface charge regulated with light illumination, together with the results of our previous work, an intensity of 50 mW/cm^2 was chosen for cell detachment. As the illumination time increased, more cells were released from the Gr/Si surface (Fig. S13a). After being illuminated for 10 min, over 90% of cells were detached from Gr/Si, while for the negative control n-Si, no significant detachment was noted (Fig. S13a and 4b). Meanwhile, the monolayer Gr film on insulated glass substrates without heterojunction could not be used as a cell retrieval platform with light illumination (Fig. S14), further confirming the above postulation. Retained cell survival and re-attachability were observed for light-detached cells compared with those digested with trypsin, showcasing the non-cytotoxicity of the Gr/Si system (Fig. 4c and d). Next, light-regulated cell adhesion behaviors were further demonstrated by the spatial control of cell detachment from Gr/Si with light illumination (Fig. S13b and S13c). As predicted, few cells were observed in the middle region (Gr/Si) while the majority were left on the edges of the substrate (bare n-Si), portraying its potential for patterned cell harvesting in the future.

Secondly, the light-activated molecular switch system was built to induce whole MC3T3-E1 sheet detachment (Fig. 4e and S15). The resultant cell sheets showed satisfactory cell viability, well-maintained cell-to-cell connection (positive E-cadherin expression), and ECM proteins (cell-adhesive glycoproteins laminin and Col-1) (Fig. 4f). After being re-cultured on another 24-well plate, cellular outgrowths from the cell sheet fragments exhibited a spreading morphology and maintained migratory capability from the detached sheets (Fig. S16). Additionally, light-harvested MC3T3-E1 cell sheets improved alkaline phosphatase (ALP) activity as a significant early marker of osteogenic differentiation rather than cells cultured on a conventional 24-well plate under the same cultivation conditions (Fig. 4g and h). Real-time polymerase chain reaction (RT-PCR) results displayed identical trends for the expression levels of early markers (ALP and Runx-2) (Fig. 4i). This enhanced osteogenic differentiation of light-harvested cell sheets should be attributed to the contribution of the stiff and large area of Gr film, which was reported to be favorable for cell adhesion, proliferation, and osteogenic differentiation [76,77].

In addition to MC3T3-E1 cells, detached living rat bone marrow mesenchymal stromal cells (rBMSCs) sheets were similarly harvested, demonstrating the repeatability of this Gr/Si system (Fig. S17). To validate the light-induced charge transfer from ECM protein to Gr/Si, the chemical status of the recycled Gr/Si surface was examined (Fig. S18). Protonated NH_3+ groups were observed on the recycled Gr/Si substrates after light-detached MC3T3-E1 and rBMSCs cell sheets, confirming the above light-driven doping process. Moreover, the upregulated integrin-β1 expression in rBMSCs cell sheets was also observed after detachment compared with undetached cell sheets on Gr/Si (Fig. S19). Both changes in integrin-β1 and ECM proteins (Figs. 2–3) in cell sheets may together contribute to light-induced cell detachments.

To elucidate cellular response to cultivation/detachment by the photovoltaic Gr/Si surface on the transcriptomic scale, RNA sequencing (RNA-seq) was performed to analyze differential gene expression of

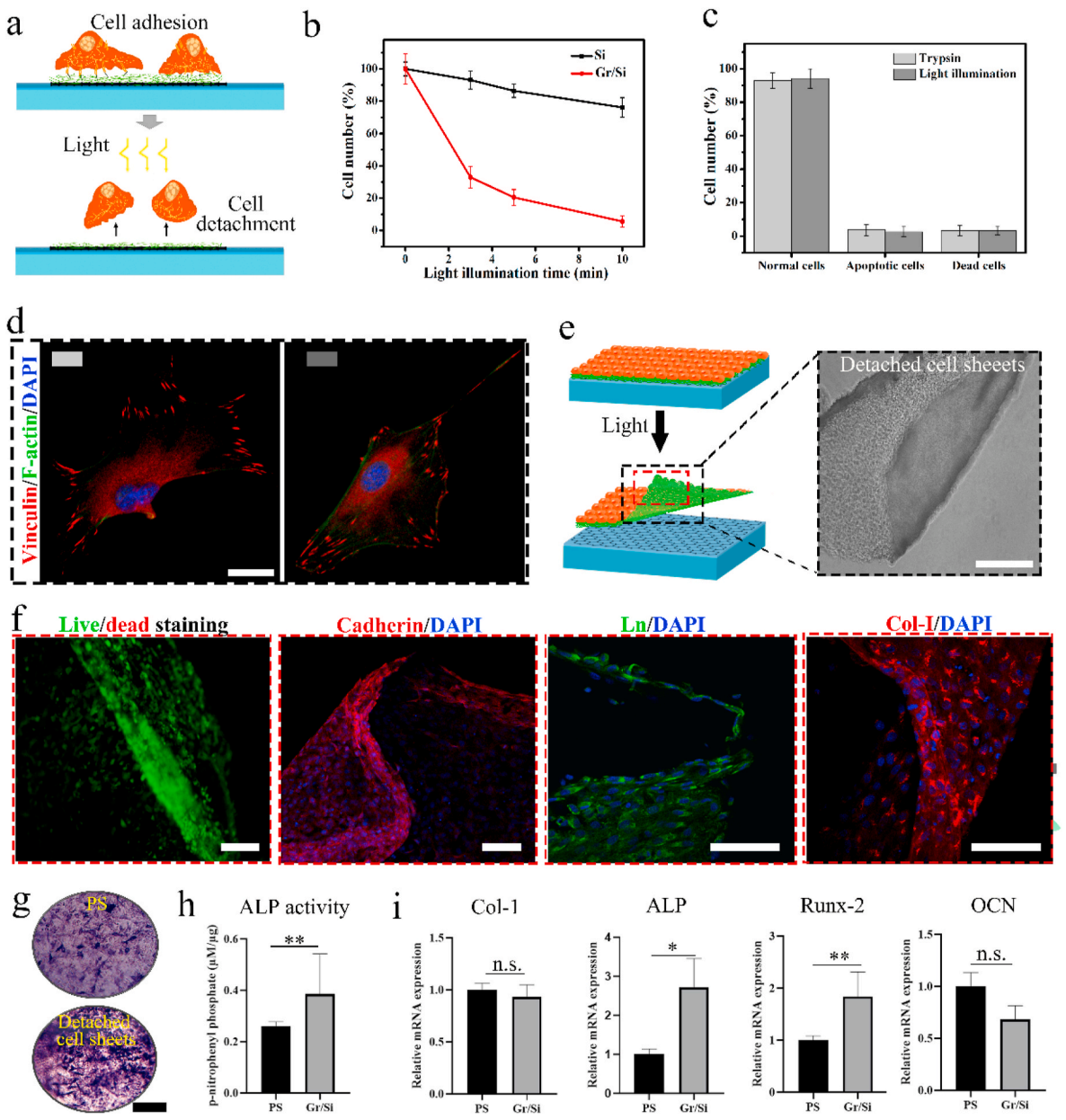

Fig. 4. Light-regulated cell detachment behaviors. (a) A schematic showing visible light-induced single cells detachment from Gr/Si surface; (b) Time courses changes in the light-induced cell detachment ratios. Bare n-Si substrates were used as control; (c) Viability of detached cells assessed by flow cytometry; (d) Confocal images showing cell morphology of reseeded cells detached by trypsin treatments (left) and light illumination (right); (e) Schematics of light-induced cell sheets detachment from Gr/Si. The microscopic image in the dashed box was light harvested cell sheets; (f) Fluorescent images showing cell viability, cell-to-cell connection, and retained ECM proteins of detached cell sheets; (g–h) ALP activity of light harvested cell sheets. Cell sheets cultured on PS culture plates were used as control. (i) Osteogenesis-related gene expressions (ALP, Runx-2, Col-1, and OCN) of harvested cell sheets, compared with cells cultured on PS plate. $^{*}p < 0.05$, $^{**}p < 0.01$. The model cell was MC3T3-E1. Scale bar in d = 20 μm, in e and g = 200 μm, in f = 100 μm.

rBMSCs harvested from the PS plate and Gr/Si system before and after light treatment (Supplementary file 1, Fig. 5). Principal component analysis (PCA) revealed a clear separation between cells cultured on Gr/Si and the PS plate when projected on the first two principal components, while cell sheets on Gr/Si treated before and after light-induced cell detachment were closer to each other (Fig. 5a). Meanwhile, only 15 differentially expressed genes were identified from rBMSCs cell sheets detached from Gr/Si, compared with the undetached cell sheets on Gr/Si (Fig. S20). When compared with cells on the PS plate, 1079 DEGs, including 676 upregulated and 420 downregulated ones, were identified from cell sheets detached from Gr/Si with light illumination (Fig. 5b and c). These results indicated Gr/Si surface rather than light treatment contributed to the gene expression pattern alterations of BMSCs. Gene ontology (GO) analysis determined that bone remodeling, cell-substrate adhesion, macrophage activation as well as wound healing-associated genes were over-represented in the light-harvested cell sheets (Fig. 5d), suggesting their potential application in wound healing and bone regeneration. Enrichment of GO terms related to macrophage activation and downstream effect in response to interleukin-1 in light-harvested BMSCs (Fig. 5e) imply that Gr/Si surface may show a positive effect on the immunoregulatory property of BMSCs [78]. Enriched KEGG pathways as the notch and PI3K-Akt signaling pathways and focal adhesion were reported to promote rBMSC osteogenesis (Fig. 5f) [79,80]. Moreover, we compared the osteogenic gene expression patterns in rBMSCs cell sheets culturing on Gr/Si and detached from Gr/Si in a light-regulated manner (Fig. S21), and the results

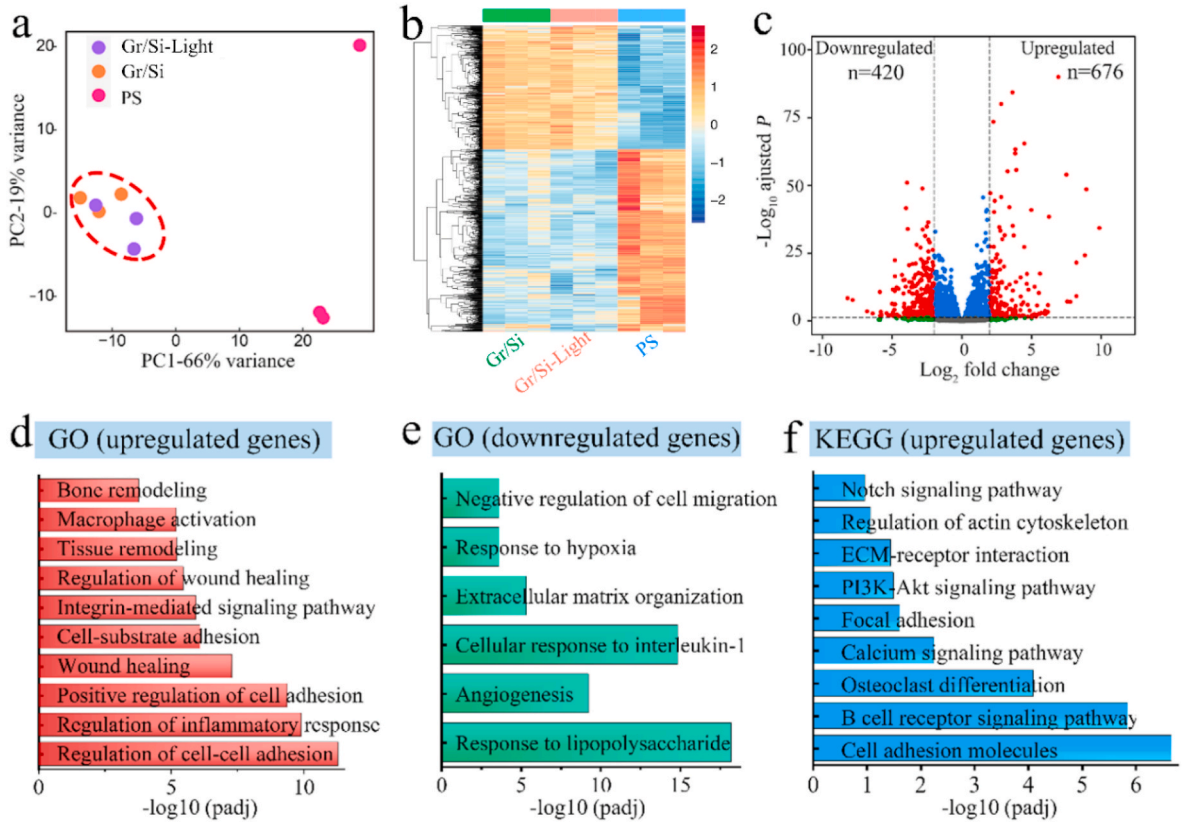

Fig. 5. RNA-sequencing of light-harvested rBMSCs cell sheets. (a) PCA of RNA-seq expression profile was obtained for cell sheets on Gr/Si before and after detachment, and cell sheets on PS were used as control. (b) The heatmap of differentially expressed genes from RNA-seq analysis was performed on rBMSCs cell sheets on Gr/Si before (Gr/Si) and after light-induced detachment (Gr/Si-Light) and cell sheets cultured on PS plate. (c) Volcano plot of differentially expressed genes from RNA-seq analysis performed on light-harvested rBMSCs cell sheets and cells cultured on PS plate. (d) and (e) are gene ontology (GO) enrichment analyses of the up- and down-regulated genes in rBMSCs cell sheets cultured on the Gr/Si system, respectively. (f) The KEGG pathway analysis of upregulated genes in rBMSCs cell sheets cultured on Gr/Si system.

showed no significant difference in gene expressions between them. We have also examined the osteogenic gene expression patterns of rBMSCs cell sheets on Gr/Si (before detachment) and PS (Fig. S22). Upregulated osteogenic genes were found in rBMSCs cell sheets on Gr/Si surface than PS, further consolidating that Gr film rather than light treatment contributed to the promoted osteogenic properties of rBMSCs cell sheets. Taken together, rBMSCs or MC3T3-E1 cell sheets cultured and harvested from Gr/Si surfaces may retain higher osteogenic potential, making them ideal for bone tissue regeneration in the future.

Considering the above results, the mechanism for light-induced cell detachment from the Gr/Si surface could be (Fig. 6): upon light illumination, electrons in Gr were energetically transferred to the Si side due to the existence of the built-in field (Fig. 1), leading to holes retained in the Gr side to achieve positive charge accumulation, thereby ECM protein molecules atop Gr underwent protonation to provide negative charges for Gr by π-π interactions (Figs. 2 and 3); this charge transfer could further induce conformational changes of the ECM protein adsorbed (Fig. 3), which would, in turn, facilitate the charge transfer process; this process also influences the expression of integrin-β1 in cell sheets (Fig. S19); both changes in ECM proteins and integrin-β1 in cells together weaken the binding sites between Fn (like RGD) and integrin (α5β1, not limited) [81], and eventually induce cell detachment (Figs. 4 and 5).

Substrate stiffness differentially regulates cell differentiation, and

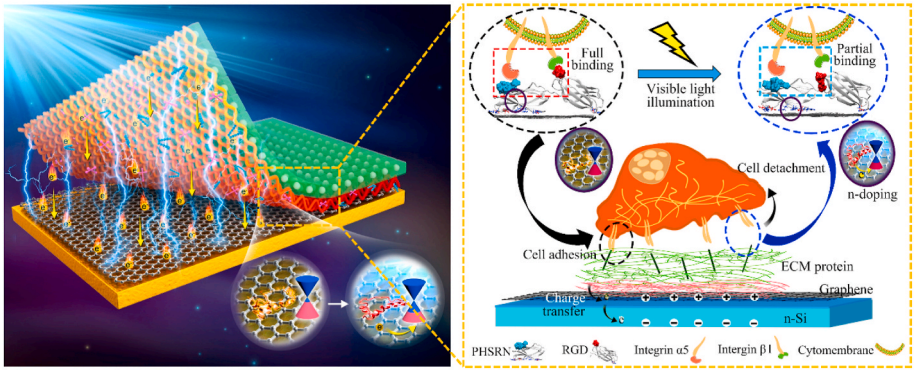

Fig. 6. Schematic illustration showing light-harnessed charge transfer from ECM protein to Gr/Si via the photovoltaic interface for efficient cell detachment.

MSCs on stiff substrates abet osteogenesis [76,77,82]. Stiff and large-area graphene surfaces in our system contribute to the osteogenesis of rBMSCs, which own great potential in bone tissue engineering. However, compared with tunable extracellular matrix (e.g. adaptable hydrogel), the Gr/Si interface may be not adaptable for cells toward adipogenesis and chondrogenesis [83]. Although magnetic field-mediated nanoplate and nano-assembly by tuning the binding of integrin to RGDs could promote focal adhesion, mechanotransduction, and differentiation of stem cells in a reversible manner [84,85], the off-target effects and low reproducibility of "nano-magnetic particles" remain challenging [86]. In this regard, the Gr/Si system owned a simple and homogeneous surface, capable of large-scale production of reproducible photovoltaic substrates for biomedical applications.

On the other hand, remarkable works have been made in azobenzene-based *cis-trans* photo-isomerizable design and synthesis, depending on the chemical modification of its structure [13,87,88]. Nevertheless, the introduction of free chemicals may have an additional effect on protein conformation and cellular responses as well [89]. To diminish such risk, in this Gr/Si system, visible light illumination regulated charge transfer from ECM proteins to Gr/Si could directly mediate the interaction between cell surface receptor-RGD/PHSRN ligand and integrin-β1 [90]. The entire process enables safe and controllable cell detachment. Moreover, compared with previously developed Si(p/n) system which regulated cell adhesion by light-induced electron accumulation [20], the positively charged surface in Gr/Si system varyingly interacts with cells, further providing an effective pathway to tailor the cellular responses.

4. Conclusion

Visible light-controlled cell adhesion/detachment based on Gr/Si has been achieved by regulating the dynamic protein-Gr interactions. Upon light illumination, positive charge accumulated and promoted charge transfer between the surface and ECM protein molecules, resulting in conformational changes in the proteins. Such dynamic regulation through light illumination showed opposite effects on the stable cell adhesion states and eventually realized noninvasive cell detachment. This fundamental work not only provides a method for dynamically regulating cell adhesion behaviors but also shows promising potential for developing more powerful tools in tissue engineering and regeneration.

Ethics approval and consent to participate

Sprague-Dawley rats (SD rats) were provided by Laboratory Animal Center of Zhejiang University. All experimental protocols were approved by the Institutional Animal Care and Use Committee of Zhejiang University, Hangzhou, China. All animals received humane care according to the criteria of Guide for the Care and Use of Laboratory Animals.

CRediT authorship contribution statement

Xiaozhao Wang: contributed equally to this work, Formal analysis, Methodology, Writing – original draft, Funding acquisition. **Cai Yao:** contributed equally to this work, MD simulation, Writing – original draft. **Xudong Yao:** contributed equally to this work, Formal analysis, Writing – original draft. **Junxin Lin:** Methodology, Writing – original draft. **Rui Li:** Formal analysis, Methodology. **Kun Huang:** Methodology. **Weiming Lin:** Methodology. **Xiaojun Long:** Methodology. **Chao Dai:** Methodology. **Jiajun Dong:** Methodology. **Xuegong Yu:** Methodology. **Wenwen Huang:** Formal analysis, Methodology. **Wenjian Weng:** Conceptualization, Writing – original draft. **Qi Wang:** MD simulation. **Hongwei Ouyang:** Conceptualization, Formal analysis, Writing – original draft. **Kui Cheng:** Conceptualization, Formal analysis, Writing – original draft, Funding acquisition.

Declaration of competing interest

The authors declare no conflict of interest.

Acknowledgments

X.W., C.Y., and X.Y. contributed equally to this work. The National Key R&D Program of China (2021YFC2400400), the National Science Foundation of China (52072339, 21673206 and 82002271) financially supported this work. Computing resources were provided by ScGrid http://www.cngrid.org and the Guangzhou National Supercomputer Center (NSCC-GZ). We thank Dr. Zhengzhong Kang for his helpful discussion in the MD simulation.

Appendix A. Supplementary data

Supplementary data to this article can be found online at https://doi.org/10.1016/j.bioactmat.2022.09.022.

References

[1] J.Z. Kechagia, J. Ivaska, P. Roca-Cusachs, Integrins as biomechanical sensors of the microenvironment, Nat. Rev. Mol. Cell Biol. 20 (2019) 457–473, https://doi.org/10.1038/s41580-019-0134-2.
[2] T.T. Lee, J.R. García, J.I. Paez, A. Singh, E.A. Phelps, S. Weis, Z. Shafiq, A. Shekaran, A. Del Campo, A.J. J.N.m. García, Light-triggered in vivo activation of adhesive peptides regulates cell adhesion, inflammation and vascularization of biomaterials, Nat. Mater. 14 (2015) 352–360, https://doi.org/10.1038/nmat4157.
[3] W.L. Murphy, T.C. McDevitt, A.J. Engler, Materials as stem cell regulators, Nat. Mater. 13 (2014) 547–557, https://doi.org/10.1038/nmat3937.
[4] B. Geiger, J.P. Spatz, A.D. Bershadsky, Environmental sensing through focal adhesions, Nat. Rev. Mol. Cell Biol. 10 (2009) 21–33, https://doi.org/10.1038/nrm2593.
[5] J. Robertus, W.R. Browne, BenL. Feringa, Dynamic control over cell adhesive properties using molecular-based surface engineering strategies, Chem. Soc. 39 (2010) 354–378, https://doi.org/10.1039/B906608J.
[6] Q. Liu, C. Wu, H. Cai, N. Hu, J. Zhou, P.J. C.r. Wang, Cell-based biosensors and their application in biomedicine, Chem. Rev. 114 (2014) 6423–6461, https://doi.org/10.1021/cr2003129.
[7] J. Kim, W.A. Li, Y. Choi, S.A. Lewin, C.S. Verbeke, G. Dranoff, D. J. Mooney Injectable, Spontaneously assembling, inorganic scaffolds modulate immune cells in vivo and increase vaccine efficacy, Nat. Biotechnol. 33 (2015) 64–72, https://doi.org/10.1038/nbt.3071.
[8] O.A. Ali, N. Huebsch, L. Cao, G. Dranoff, David J. Mooney, Infection-mimicking materials to program dendritic cells in situ, Nat. Mater. 8 (2009) 151–158, https://doi.org/10.1038/nmat2357.
[9] Y. Ma, X. Tian, L. Liu, J. Pan, G. Pan, Dynamic synthetic biointerfaces: from reversible chemical interactions to tunable biological effects, Acc. Chem. Res. 52 (2019) 1611–1622, https://doi.org/10.1021/acs.accounts.8b00604.
[10] J.D. Kim, J.S. Heo, T. Park, C. Park, H.O. Kim, Eunkyoung Kim, Photothermally induced local dissociation of collagens for harvesting of cell sheets, Angew. Chem. 20 (2015) 5869–5873, https://doi.org/10.1002/anie.201411386.
[11] W. Li, J. Wang, J. Ren, Xiaogang Qu, Near-infrared upconversion controls photocaged cell adhesion, J. Am. Chem. Soc. 6 (2014) 2248–2251, https://doi.org/10.1021/ja412364m.
[12] H. Liu, Y. Li, K. Sun, J. Fan, P. Zhang, J. Meng, S. Wang, L. Jiang, Dual-responsive surfaces modified with phenylboronic acid-containing polymer brush to reversibly capture and release cancer cells, J. Am. Chem. Soc. 20 (2013) 7603–7609, https://doi.org/10.1021/ja401000m.
[13] W. Li, Z. Chen, L. Zhou, Z. Li, J. Ren, X. J. J. o. t. A. C. S. Qu, Noninvasive and reversible cell adhesion and detachment via single-wavelength near-infrared laser mediated photoisomerization, J. Am. Chem. Soc. 25 (2015) 8199–8205, https://doi.org/10.1021/jacs.5b03872.
[14] M. Wirkner, J.M. Alonso, V. Maus, M. Salierno, T.T. Lee, A.J. García, A. del Campo, Triggered cell release from materials using bioadhesive photocleavable linkers, Adv. Mater. 23 (2011) 3907–3910, https://doi.org/10.1002/adma.201100925.
[15] J. You, J.S. Heo, J. Kim, T. Park, B. Kim, H.-S. Kim, Y. Choi, H.O. Kim, E. J. A. n. Kim, Noninvasive photodetachment of stem cells on tunable conductive polymer nano thin films: selective harvesting and preserved differentiation capacity, ACS Nano 7 (2013) 4119–4128, https://doi.org/10.1021/nn400405t.
[16] L.F. Kadem, M. Holz, K.G. Suana, Q. Li, C. Lamprecht, R. Herges, C. J. A. M. Selhuber-Unkel, Rapid reversible photoswitching of integrin-mediated adhesion at the single-cell level, Adv. Mater. 9 (2016) 1799–1802, https://doi.org/10.1002/adma.201504394.
[17] J. Nicolas, S. Magli, L. Rabbachin, S. Sampaolesi, F. Nicotra, L. Russo, 3d extracellular matrix mimics: fundamental concepts and role of materials chemistry to influence stem cell fate, Biomacromolecules 21 (2020) 1968–1994, https://doi.org/10.1021/acs.biomac.0c00045.

[18] J.J. Giner-Casares, M. Henriksen-Lacey, I. García, L. M. J. A. C. I. E. Marzán, Plasmonic surfaces for cell growth and retrieval triggered by near-infrared light, Angew. Chem. 3 (2016) 974–978, https://doi.org/10.1002/anie.201509025.

[19] T.A. Kolesnikova, D. Kohler, A.G. Skirtach, H.J. A.n. Mohwald, Laser-induced cell detachment, patterning, and regrowth on gold nanoparticle functionalized surfaces, ACS Nano 6 (2012) 9585–9595, https://doi.org/10.1021/nn302891u.

[20] X. Wang, C. Yao, W. Weng, K. Cheng, Q. J. A. a. m. Wang, interfaces. Visible-light-responsive surfaces for efficient, noninvasive cell sheet harvesting, ACS Appl. Mater. Interfaces 9 (2017) 28250–28259, https://doi.org/10.1021/acsami.7b08868.

[21] S. Guo, X. Zhu, M. Li, L. Shi, J.L.T. Ong, D. Jańczewski, K. G. J. A. a. m. Neoh, interfaces. Parallel control over surface charge and wettability using polyelectrolyte architecture: effect on protein adsorption and cell adhesion, ACS Appl. Mater. Interfaces 8 (2016) 30552–30563, https://doi.org/10.1021/acsami.6b09481.

[22] A.M.D. Wan, R.M. Schur, C.K. Ober, C. Fischbach, D. Gourdon, G.G. Malliaras, Electrical control of protein conformation, Adv. Mater. 24 (2012) 2501–2505, https://doi.org/10.1002/adma.201200436.

[23] K. Cheng, Y. Hong, M. Yu, J. Lin, W. Weng, H.J. S.r. Wang, Modulation of protein behavior through light responses of tio2 nanodots films, Sci. Rep. 5 (2015) 1–7, https://doi.org/10.1038/srep13354.

[24] Y. Chen, E.R. Cruz-Chu, J.C. Woodard, M.R. Gartia, K. Schulten, L. J. A. n. Liu, Electrically induced conformational change of peptides on metallic nanosurfaces, ACS Nano 6 (2012) 8847–8856, https://doi.org/10.1021/nn3027408.

[25] M. Lashkor, F.J. Rawson, A. Stephenson-Brown, J.A. Preece, P. Mendes, Electrically-driven modulation of surface-grafted rgd peptides for manipulation of cell adhesion, Chem. Commun. 50 (2014) 15589–15592, https://doi.org/10.1039/C4CC06649A.

[26] S. Hertig, M. Chabria, V. Vogel, Engineering mechanosensitive multivalent receptor–ligand interactions: why the nanolinker regions of bacterial adhesins matter, Nano Lett. 12 (2012) 5162–5168, https://doi.org/10.1021/nl302153h.

[27] X. Li, H. Zhu, K. Wang, A. Cao, J. Wei, C. Li, Y. Jia, Z. Li, X. Li, D. Wu, Graphene-on-silicon Schottky junction solar cells, Adv. Mater. 22 (2010) 2743–2748, https://doi.org/10.1002/adma.200904383.

[28] S.K. Jang, J.-r. Jang, W.-S. Choe, S.J.A.A.M. Lee, Interfaces. Harnessing denatured protein for controllable bipolar doping of a monolayer graphene, ACS Appl. Mater. Interfaces 7 (2015) 1250–1256, https://doi.org/10.1021/am507246v.

[29] S. Wei, X. Zou, J. Tian, H. Huang, W. Guo, Z. Chen, Control of protein conformation and orientation on graphene, J. Am. Chem. Soc. 51 (2019) 20335–20343, https://doi.org/10.1021/jacs.9b10705.

[30] X. Zou, S. Wei, J. Jasensky, M. Xiao, Q. Wang, C.L. Brooks, Z. Chen, Molecular interactions between graphene and biological molecules, J. Am. Chem. Soc. 5 (2017) 1928–1936, https://doi.org/10.1021/jacs.6b11226.

[31] L. Zhou, K. Wang, Z. Wu, H. Dong, H. Sun, X. Cheng, H.L. Zhang, H. Zhou, C. Jia, Q. J.L. Jin, Investigation of controllable nanoscale heat-denatured bovine serum albumin films on graphene, Langmuir 32 (2016) 12623–12631, https://doi.org/10.1021/acs.langmuir.6b03296.

[32] S.S. Kwon, J.H. Shin, J. Choi, S. Nam, W.I. Park, Defect-mediated molecular interaction and charge transfer in graphene mesh-glucose sensors, ACS Appl. Mater. Interfaces 9 (2017) 14216–14221, https://doi.org/10.1021/acsami.7b00848.

[33] W.E. Gregory, B. Sharma, L. Hu, A.J. Raghavendra, R. Podila, Interfacial charge transfer with exfoliated graphene inhibits fibril formation in lysozyme amyloid, Biointerphases 15 (2020), 031010, https://doi.org/10.1116/6.0000019.

[34] M. Kim, N.S. Safron, C. Huang, M.S. Arnold, P.J. N.l. Gopalan, Light-driven reversible modulation of doping in graphene, Nano Lett. 12 (2012) 182–187, https://doi.org/10.1021/nl2032734.

[35] X. Long, X. Wang, L. Yao, S. Lin, J. Zhang, W. Weng, K. Cheng, H. Wang, J. Lin, Graphene/si-promoted osteogenic differentiation of bmscs through light illumination, ACS Appl. Mater. Interfaces 11 (2019) 43857–43864, https://doi.org/10.1021/acsami.9b14679.

[36] S. Picelli, Å.K. Björklund, O.R. Faridani, S. Sagasser, G. Winberg, R. Sandberg, Smart-seq2 for sensitive full-length transcriptome profiling in single cells, Nat. Methods 10 (2013) 1096–1098, https://doi.org/10.1038/nmeth.2639.

[37] Y. Henrotin, L. Pesesse, C. Sanchez, Subchondral bone and osteoarthritis: biological and cellular aspects, Osteoporos. Int. 23 (2012) 847–851, https://doi.org/10.1007/s00198-012-2162-z.

[38] J. Li, F. Wang, Water graphene contact surface investigated by pairwise potentials from force-matching paw-pbe with dispersion correction, J. Chem. Phys. 5 (2017), 054702, https://doi.org/10.1063/1.4974921.

[39] J.O.M. Bockris, M.A.V. Devanathan, K. Müller, On the Structure of Charged Interfaces, Proc Roy. Soc., A. Pergamon, 1965, pp. 832–863.

[40] A. Bujacz, Structures of bovine, equine and leporine serum albumin, Acta Crystallogr. D 68 (2012) 1278–1289, https://doi.org/10.1107/S0907444912027047.

[41] D.J. Leahy, I. Aukhil, H.P. Erickson, 2.0 Å crystal structure of a four-domain segment of human fibronectin encompassing the rgd loop and synergy region, Cell 84 (1996) 155–164, https://doi.org/10.1016/S0092-8674(00)81002-8.

[42] D. Van Der Spoel, E. Lindahl, B. Hess, G. Groenhof, A.E. Mark, H.J.C. Berendsen, Gromacs: fast, flexible, and free, J. Comput. Chem. 26 (2005) 1701–1718, https://doi.org/10.1002/jcc.20291.

[43] K. Lindorff-Larsen, S. Piana, K. Palmo, P. Maragakis, J.L. Klepeis, R.O. Dror, D. E. Shaw, Improved side-chain torsion potentials for the amber ff99sb protein force field, Proteins: Struct., Funct., Bioinf. 78 (2010) 1950–1958, https://doi.org/10.1002/prot.22711.

[44] B. Hess, H. Bekker, H.J.C. Berendsen, J. G. E. M. Fraaije. Lincs, A linear constraint solver for molecular simulations, J. Comput. Chem. 18 (1997) 1463–1472, https://doi.org/10.1002/(SICI)1096-987X(199709)18:12<1463::AID-JCC4>3.0.CO;2-H.

[45] T. Darden, D. York, L. Pedersen, Particle mesh ewald: an log(n) method for ewald sums in large systems, J. Chem. Phys. 12 (1993) 10089–10092, https://doi.org/10.1063/1.464397.

[46] J.W. Suk, W.H. Lee, J. Lee, H. Chou, R.D. Piner, Y. Hao, D. Akinwande, R.S. J.N. l. Ruoff, Enhancement of the electrical properties of graphene grown by chemical vapor deposition via controlling the effects of polymer residue, Nano Lett. 13 (2013) 1462–1467, https://doi.org/10.1021/nl304420b.

[47] A.C. Ferrari, J.C. Meyer, V. Scardaci, C. Casiraghi, M. Lazzeri, F. Mauri, S. Piscanec, D. Jiang, K.S. Novoselov, S. Roth, A.K. Geim, Raman spectrum of graphene and graphene layers, Phys. Rev. Lett. 97 (2006), 187401, https://doi.org/10.1103/PhysRevLett.97.187401.

[48] C. Casiraghi, S. Pisana, K.S. Novoselov, A.K. Geim, A.C. Ferrari, Raman fingerprint of charged impurities in graphene, Appl. Phys. Lett. 91 (2007), 233108, https://doi.org/10.1063/1.2818692.

[49] S. Jung, J. Lee, J. Seo, U. Kim, Y. Choi, H. Park, Development of annealing-free, solution-processable inverted organic solar cells with n-doped graphene electrodes using zinc oxide nanoparticles, Nano Lett. 18 (2018) 1337–1343, https://doi.org/10.1021/acs.nanolett.7b05026, 2018.

[50] B. Luan, T. Huynh, L. Zhao, R. Zhou, Potential toxicity of graphene to cell functions via disrupting protein-protein interactions, ACS Nano 9 (2015) 663–669, https://doi.org/10.1021/nn506011j.

[51] D. Sinha, J.U. Lee, Ideal graphene/silicon Schottky junction diodes, Nano Lett. 14 (2014) 4660–4664, https://doi.org/10.1021/nl501735k.

[52] Y. Hong, M. Yu, W. Weng, K. Cheng, H. Wang, J.J.B. Lin, Light-induced cell detachment for cell sheet technology, Biomaterials 34 (2013) 11–18, https://doi.org/10.1016/j.biomaterials.2012.09.043.

[53] D.C. Carter, J. X. J. A. i. p. c. Ho, Structure of serum albumin, Adv. Protein Chem. 45 (1994) 153–203, https://doi.org/10.1016/S0065-3233(08)60640-3.

[54] Y. Mulyana, M. Uenuma, N. Okamoto, Y. Ishikawa, I. Yamashita, Y.J.A.A. M. Uraoka, Interfaces. Creating reversible p-n junction on graphene through ferritin adsorption, ACS Appl. Mater. Interfaces 8 (2016) 8192–8200, https://doi.org/10.1021/acsami.5b12226.

[55] S.K. Jang, J.-r. Jang, W.-S. Choe, S. Lee, Harnessing denatured protein for controllable bipolar doping of a monolayer graphene, ACS Appl. Mater. Interfaces 7 (2015) 1250–1256, https://doi.org/10.1021/am507246v.

[56] A. Das, S. Pisana, B. Chakraborty, S. Piscanec, S.K. Saha, U.V. Waghmare, K. S. Novoselov, H.R. Krishnamurthy, A.K. Geim, A.C. Ferrari, A.K. Sood, Monitoring dopants by Raman scattering in an electrochemically top-gated graphene transistor, Nat. Nanotechnol. 3 (2008) 210–215, https://doi.org/10.1038/nnano.2008.67.

[57] B. Das, R. Voggu, C.S. Rout, C.N.R. Rao, Changes in the electronic structure and properties of graphene induced by molecular charge-transfer, Chem. Commun. 41 (2008) 5155–5157, https://doi.org/10.1039/B808955H.

[58] S.N. Kim, Z. Kuang, J.M. Slocik, S.E. Jones, Y. Cui, B.L. Farmer, M.C. McAlpine, R. R. J. J. o. t. A. C. S. Naik, Preferential binding of peptides to graphene edges and planes, J. Am. Chem. Soc. 133 (2011) 14480–14483, https://doi.org/10.1021/ja2042832.

[59] M.S. Mannoor, H. Tao, J.D. Clayton, A. Sengupta, D.L. Kaplan, R.R. Naik, N. Verma, F.G. Omenetto, M.C. J.N.c. McAlpine, Graphene-based wireless bacteria detection on tooth enamel, Nat. Commun. 3 (2012) 1–9, https://doi.org/10.1038/ncomms1767.

[60] G.S. Longo, I. J. J. o. P. D. A. P. Szleifer, Adsorption and protonation of peptides and proteins in ph responsive gels, J. Phys. D Appl. Phys. 49 (2016) 323001–3230016, https://doi.org/10.1088/0022-3727/49/32/323001.

[61] R. Podila, P. Vedantam, P. Ke, J. Brown, A. Rao, Evidence for charge-transfer-induced conformational changes in carbon nanostructure-protein corona, J. Phys. Chem. C 116 (2012) 22098–22103, https://doi.org/10.1021/jp3085028.

[62] K. Belbachir, R. Noreen, G. Gouspillou, C.J.A. Petibois, b. chemistry. Collagen types analysis and differentiation by ftir spectroscopy, Anal. Bioanal. Chem. 395 (2009) 829–837, https://doi.org/10.1007/s00216-009-3019-y.

[63] C. Mücksch, H.M. Urbassek, Molecular dynamics simulation of free and forced bsa adsorption on a hydrophobic graphite surface, Langmuir 27 (2011) 12938–12943, https://doi.org/10.1021/la201972f.

[64] P. Hampitak, D. Melendrez, M. Iliut, M. Fresquet, N. Parsons, B. Spencer, T. A. Jowitt, A. Vijayaraghavan, Protein interactions and conformations on graphene-based materials mapped using a quartz-crystal microbalance with dissipation monitoring (qcm-d), Carbon 165 (2011) 317–327, https://doi.org/10.1016/j.carbon.2020.04.093.

[65] Z. Huang, Y. Zhao, B. Liu, S. Guan, J. Liu, Stronger adsorption of phosphorothioate DNA oligonucleotides on graphene oxide by van der waals forces, Langmuir 36 (2020) 13708–13715, https://doi.org/10.1021/acs.langmuir.0c02761.

[66] J. Katoch, S.N. Kim, Z. Kuang, B.L. Farmer, R.R. Naik, S.A. Tatulian, M.J. N. l. Ishigami, Structure of a peptide adsorbed on graphene and graphite, Nano Lett. 12 (2012) 2342–2346, https://doi.org/10.1021/nl300286k.

[67] J. Guo, X. Yao, L. Ning, Q. Wang, H.J.R.A. Liu, The adsorption mechanism and induced conformational changes of three typical proteins with different secondary structural features on graphene, RSC Adv. 4 (2014) 9953–9962, https://doi.org/10.1039/C3RA45876H.

[68] B. Haylee, N. John, D. Marilyn, H.B. Thomas, Utilizing fibronectin integrin-binding specificity to control cellular responses, Adv. Wound Care 4 (2015) 501–511, https://doi.org/10.1089/wound.2014.0621.

[69] T. Li, L. Hao, J. Li, C. Du, Y. Wang, Role of ninth type-iii domain of fibronectin in the mediation of cell-binding domain adsorption on surfaces with different

chemistries, Langmuir 34 (2018) 9847–9855, https://doi.org/10.1021/acs.langmuir.8b01937, 2018.
[70] S. Basu, B. Gorai, B. Basu, P.K. Maiti, Electric field-mediated fibronectin–hydroxyapatite interaction: a molecular insight, J. Phys. Chem. B 125 (2021) 3–16, https://doi.org/10.1021/acs.jpcb.0c08255.
[71] S.E. Stabenfeldt, A.C. Brown, T.H. Barker, Engineering ECM Complexity into Biomaterials for Directing Cell Fate. Biomaterials as Stem Cell Niche, Springer, Berlin, 2010, pp. 1–18.
[72] B. Tang, J. Zhuang, L. Wang, B. Zhang, S. Lin, F. Jia, L. Dong, Q. Wang, K. Cheng, W. J. A. a. m. Weng, Harnessing cell dynamic responses on magnetoelectric nanocomposite films to promote osteogenic differentiation, ACS Appl. Mater. Interfaces 10 (2018) 7841–7851, https://doi.org/10.1021/acsami.7b19385, interfaces.
[73] S.E. Ochsenhirt, E. Kokkoli, J.B. McCarthy, M.J.B. Tirrell, Effect of rgd secondary structure and the synergy site phsrn on cell adhesion, spreading and specific integrin engagement, Biomaterials 27 (2006) 3863–3874, https://doi.org/10.1016/j.biomaterials.2005.12.012.
[74] C. Brakebusch, R.J.C. Fässler, M. Reviews, β 1 integrin function in vivo: adhesion, migration and more, Cancer Metastasis Rev. 24 (2005) 403–411, https://doi.org/10.1007/s10555-005-5132-5.
[75] B. Akdim, R. Pachter, S.S. Kim, R.R. Naik, T.R. Walsh, S. Trohalaki, G. Hong, Z. Kuang, B. L. J. A. a. m. Farmer, Electronic properties of a graphene device with peptide adsorption: insight from simulation, ACS Appl. Mater. Interfaces 5 (2013) 7470–7477, https://doi.org/10.1021/am401731c, interfaces.
[76] W.C. Lee, C.H.Y.X. Lim, H. Shi, L.A.L. Tang, Y. Wang, C.T. Lim, K.P. Loh, Origin of enhanced stem cell growth and differentiation on graphene and graphene oxide, ACS Nano 5 (2011) 7334–7341, https://doi.org/10.1021/nn202190c.
[77] T.R. Nayak, H. Andersen, V.S. Makam, C. Khaw, S. Bae, X. Xu, P.-L.R. Ee, J.-H. Ahn, B.H. Hong, G. Pastorin, B. Özyilmaz, Graphene for controlled and accelerated osteogenic differentiation of human mesenchymal stem cells, ACS Nano 5 (2011) 4670–4678, https://doi.org/10.1021/nn200500h.
[78] Y. Zhu, H. Liang, X. Liu, J. Wu, C. Yang, T.M. Wong, , K. Y. H. Kwan, K.M. C. Cheung, S. Wu, K. W. K. Yeung, Regulation of macrophage polarization through surface topography design to facilitate implant-to-bone osteointegration, Sci. Adv. 7 (2021) 6654–6666, https://doi.org/10.1126/sciadv.abf6654.
[79] B.C. Heng, Y. Bai, X. Li, Y. Meng, X. Zhang, X. Deng, Signaling pathways implicated in enhanced stem/progenitor cell differentiation on electroactive scaffolds, Smart Mater. Med. 3 (2022) 4–11, https://doi.org/10.1016/j.smaim.2021.11.003.
[80] B. Chang, C. Ma, X. Liu, Nanofibers regulate single bone marrow stem cell osteogenesis via fak/rhoa/yap1 pathway, ACS Appl. Mater. Interfaces 10 (2018) 33022–33031, https://doi.org/10.1021/acsami.8b11449.
[81] F. Jia, S. Lin, X. He, J. Zhang, S. Shen, Z. Wang, B. Tang, C. Li, Y. Wu, L. Dong, K. Cheng, W. Weng, Comprehensive evaluation of surface potential characteristics on mesenchymal stem cells' osteogenic differentiation, ACS Appl. Mater. Interfaces 11 (2019) 22218–22227, https://doi.org/10.1021/acsami.9b07161.
[82] S. Dupont, L. Morsut, M. Aragona, E. Enzo, S. Giulitti, M. Cordenonsi, F. Zanconato, J. Le Digabel, M. Forcato, S. Bicciato, N. Elvassore, S. Piccolo, Role of YAP/TAZ in mechanotransduction, Nature 474 (2011) 179–183, https://doi.org/10.1038/nature10137.
[83] Z. Tong, L. Jin, J.M. Oliveira, R.L. Reis, Q. Zhong, Z. Mao, C. Gao, Adaptable hydrogel with reversible linkages for regenerative medicine: dynamic mechanical microenvironment for cells, Bioact. Mater. 6 (2021) 1375–1387, https://doi.org/10.1016/j.bioactmat.2020.10.029.
[84] H. Hong, S. Min, S. Koo, Y. Lee, J. Yoon, W.Y. Jang, N. Kang, R. Thangam, H. Choi, H.J. Jung, S.-B. Han, Q. Wei, S.-H. Yu, D.-H. Kim, R. Paulmurugan, W.K. Jeong, K.-B. Lee, T. Hyeon, D. Kim, H. Kang, Dynamic ligand screening by magnetic nanoassembly modulates stem cell differentiation, Adv. Mater. 34 (2022) 2105460–2105472, https://doi.org/10.1002/adma.202105460.
[85] G. Bae, M.S. Kim, R. Thangam, T.M. Koo, W.Y. Jang, J. Yoon, S.-B. Han, L. Yang, S. Y. Kim, N. Kang, S. Min, H. Hong, H.E. Fu, M.J. Ko, D.-H. Kim, W.K. Jeong, D.-H. Kim, T.-H. Kim, J.-W. Choi, K.-B. Lee, R. Paulmurugan, Y. Zhu, H.-J. Kim, J. Lee, J.S. Kim, A. Khademhosseini, Y.K. Kim, H. Kang, Receptor-level proximity and fastening of ligands modulates stem cell differentiation, Adv. Funct. Mater. 32 (2022) 2200828–2200831, https://doi.org/10.1002/adfm.202200828.
[86] S. Del Sol-Fernández, P. Martínez-Vicente, P. Gomollón-Zueco, C. Castro-Hinojosa, L. Gutiérrez, R.M. Fratila, M. Moros, Magnetogenetics: remote activation of cellular functions triggered by magnetic switches, Nanoscale 14 (2022) 2091–2118, https://doi.org/10.1039/D1NR06303K.
[87] M.-M. Russew, S. Hecht, Photoswitches: from molecules to materials, Adv. Mater. 22 (2010) 3348–3360, https://doi.org/10.1002/adma.200904102.
[88] Y. Kim, H. Choi, J.E. Shin, G. Bae, R. Thangam, H. Kang, Remote active control of nanoengineered materials for dynamic nanobiomedical engineering, View 1 (2020) 20200029–20200051, https://doi.org/10.1002/VIW.20200029.
[89] R. Duan, D. Wu, L. Tang, X. Hu, L. Cheng, H. Yang, H. Li, F. Geng, Interactions of the cis and trans states of an azobenzene photoswitch with lysozyme induced by red and blue light, Spectrochim. Acta, Part A 229 (2020) 117965–117972, https://doi.org/10.1016/j.saa.2019.117965.
[90] J.-H. Lin, H.-Y. Chang, W.-L. Kao, K.-Y. Lin, H.-Y. Liao, Y.-W. You, Y.-T. Kuo, D.-Y. Kuo, K.-J. Chu, Y.-H. Chu, J.-J. Shyue, Effect of surface potential on extracellular matrix protein adsorption, Langmuir 30 (2014) 10328–10335, https://doi.org/10.1021/la5020362.